atmosphere

MDPI

Article

Spatiotemporal Changes in Water Yield Function and Its Influencing Factors in the Tibetan Plateau in the Past 20 Years

Lingfeng Lv [1], Longbin Han [2], Xin Wen [3], Huaiyong Shao [3,*] and Shuhan Liu [3]

[1] Faculty of Geographical Science, Beijing Normal University, Beijing 100091, China; lvlingfeng@stu.cdut.edu.cn
[2] School of Earth System Science, Tianjin University, Tianjin 300072, China; hlb@stu.cdut.edu.cn
[3] College of Earth Sciences, Chengdu University of Technology, Chengdu 610059, China; 202001110206@stu.cdut.edu.cn (X.W.); liushuhan@stu.cdut.edu.cn (S.L.)
* Correspondence: shaohuaiyong@cdut.edu.cn

Abstract: The Tibetan Plateau, known as the "Water Tower of Asia", has made important contributions to global climate regulation and water conservation. With global climate change and water shortages, the yield and reserves of water on the Tibetan Plateau have undergone obvious changes, and its water yield function and water conservation function have gradually attracted widespread attention. The results show that the total water yield in the past 20 years is 128,403.06 billion m^3, spatially reduced from southeast to northwest, and the interannual variation is large but increases slowly overall. The water yield capacity is higher in the areas of less than 3000 m and 3500~4500 m, and it is stronger with the increase in slope. The water yield capacity is extremely strong in the middle and north subtropical zone. Ecological zones with high water yield capacity are mostly covered with woodland and alpine meadows. The precipitation (P) is the dominant factor in the water yield function before actual evapotranspiration (AET) = 500 mm, and then the negative force of AET is enhanced. High altitude inhibits the positive effect of the normalized vegetation index (NDVI), and the water yield at altitudes of less than 3000 m shows an almost linear relationship with the leaf area index (LAI). When LAI > 0.2, the slower the slope, the higher the water yield and the lower the growth rate. The spatial distribution of P change and water yield change is consistent and significantly positively correlated; P and NDVI changes positively affected changes in water yield, while AET and LAI changes had the opposite effect. In summary, combined with topographic factors, this study emphasizes the influence of climate and vegetation changes on the spatiotemporal changes in water yield on the Tibetan Plateau, which can provide a theoretical basis for the assessment and prediction of water yield capacity and water conservation capacity in this area.

Keywords: Tibetan Plateau; InVEST model; water yield function; partition statistics; influencing factors

Citation: Lv, L.; Han, L.; Wen, X.; Shao, H.; Liu, S. Spatiotemporal Changes in Water Yield Function and Its Influencing Factors in the Tibetan Plateau in the Past 20 Years. *Atmosphere* **2023**, *14*, 925. https://doi.org/10.3390/atmos14060925

Academic Editor: Mukul Tewari

Received: 15 April 2023
Revised: 8 May 2023
Accepted: 11 May 2023
Published: 25 May 2023

1. Introduction

Ecosystem services provide human beings with a variety of service functions related to natural resources and the living environment, and the sustainable supply of these service functions lays the foundation for sustainable economic and social development [1]. The water conservation function of ecosystems occupies an important position in many ecosystem service functions, and it has gradually become a hotspot in the research of water resource utilization and recycling. Among them, the water yield service is committed to effectively regulating runoff, reducing soil erosion, optimizing the available water resources, and improving and purifying the water quality [2], which is of great significance and has a far-reaching influence in regulating the regional water cycle, improving the surface hydrological conditions, and maintaining the balance of regional ecosystems.

Against the background of global change and widespread water resource shortages, a series of global changes, such as global warming, glacier melting, precipitation change, and wetland area change, have exerted a significant impact on the yield and reserve of

water resources on the Tibetan Plateau [3]. As a typical area sensitive to global climate change and a fragile ecosystem area, the Tibetan Plateau is gradually showing problems in terms of water resources and ecology [4]. Therefore, quantitative research on the water yield function and water conservation function of the Tibetan Plateau will contribute to the protection of water resources and the environment, ecosystem maintenance, and optimization in Asia and even the world, and will also bring new opportunities and challenges to water resource management.

At present, the most commonly used water conservation assessment methods include the water balance method, the comprehensive water storage capacity method, the annual runoff method, and the hydrological model method. With the rapid development of RS and GIS technology, the hydrological model method has gradually become the mainstream method for water conservation assessment. It has the advantages of strong controllability, strong repeatability, and dynamic simulation, and has significant advantages in the study of large spatiotemporal scales [5]. The most commonly used physical models mainly include the Soil and Water Assessment Tool (SWAT) model, the TerrainLab model, and the Integrated Valuation of Ecosystem Services and Tradeoffs (InVEST) model, among which the InVEST model is widely used at home and abroad, including Africa, Europe, the United States, China, Côte d'Ivoire, and other regions [5–8]. The SWAT model divides the watershed into several hydrological response units, which is conducive to the analysis of spatial differences in water conservation, but the model's soil database does not match the domestic soil classification system, and the parameter values are uncertain [5,9]. The TerrainLab model uses the subsurface saturated flow mechanism to accurately estimate the groundwater level and soil water content and fully considers the effect of vegetation on evapotranspiration and the influence of the terrain, but does not consider the effect of wind speed and lacks water balance verification in the basin [10,11]. The InVEST model is based on the principle of water balance and comprehensively considers the effects of climate, land cover, soil properties, and terrain fluctuations [6,12,13]. For the Zhang coefficient, the model does not fully consider the heterogeneity of the regional climate and the reliability of existing calibration data [14]. Therefore, the localized calculation of the parameters of the InVEST model on the Qinghai–Tibet Plateau will be a key issue to improve the applicability and accuracy of the model in the alpine grasslands of the Qinghai–Tibet Plateau.

With the increasing attention given to the water conservation function of alpine grassland ecosystems at home and abroad, scholars have carried out a great deal of research on the factors affecting the spatiotemporal variation in water conservation in alpine grasslands from natural and man-made aspects. (i) Natural factors: First, researchers focus on climate (temperature, precipitation, and evapotranspiration) [15–19], vegetation (vegetation coverage and leaf area index) [20,21], and other single influencing factors to conduct research. The second task is to comprehensively analyze the effects of climate, vegetation, topography, and other factors on water conservation [4,7,22,23]. Studies have shown that these factors have an important impact on the water conservation of alpine grasslands. (ii) Human factors: The research mainly focuses on land use and mostly combines natural factors [24–30]. The research results show that the water conservation amount of alpine grassland and its spatiotemporal changes are the result of the combined effect of climate change and land use. Reasonable human intervention activities enable us to protect the water conservation function of alpine grasslands.

In the study of water conservation on the Tibetan Plateau, the spatiotemporal distribution of the water yield and the analysis of climatic factors are mostly carried out in a certain river basin, and there is little attention given to the spatiotemporal evolution characteristics of the water yield under different climatic types and ecological types. Moreover, the differences and regular characteristics of water yield functions under the influence of different topographic landforms are ignored [31–37]. At the same time, studies have shown that the water conservation function is the result of soil–vegetation–atmosphere system interaction, which is affected by multiple factors, such as the climate, vegetation, soil, and human activities, and the attention given to the coupling effect of climate elements and

vegetation cover changes on water conservation should be strengthened [38–40]. In view of this, this paper calculated the water yield of the Tibetan Plateau in the past 20 years through the InVEST model and combined the topographic factors to explore the driving effect on the spatiotemporal changes in the water yield of the Tibetan Plateau from the perspective of climate change and vegetation change; we then explored the distribution characteristics and regularities of the water yield under the comprehensive action, in order to deeply understand the current and future evolution patterns of the water yield of the Tibetan Plateau.

2. Materials and Methods

In this paper, the meteorological, land use, soil, watershed, and other data, as well as the data of the plant available water fraction (PAWC) obtained by pretreatment, were used to acquire the spatial distribution pattern of the water yield in the Tibetan Plateau from 2001 to 2020, by using the InVEST model's water yield module, and the temporal variation characteristics and significance of the water yield in the Tibetan Plateau were obtained by Sen-MK trend analysis [41].

Based on different terrain types, climate types, and ecological types, the influencing factors of the spatial distribution pattern of the water yield were analyzed. From the perspective of climate change and vegetation change, the correlation between the water yield and influencing factors was calculated by the partial correlation analysis method, and the effect of spatiotemporal changes in influencing factors on the spatiotemporal variation characteristics of the water yield was explored under different climatic and ecological divisions.

2.1. Study Region

The Tibetan Plateau, situated at the world's highest altitude and being the most extensive plateau in China, is known as the "roof of the world", "the third pole", and other names. It is located at latitude 26°00′~39°47′ N and longitude 73°19′~104°47′ E, with a total area of 2.615 million square kilometers. The altitude is 3000~5000 m, the average is more than 4000 m, and the whole area slopes from northwest to southeast. Spanning China and many other nations, it covers all of Tibet and parts of Qinghai, Xinjiang, Gansu, Sichuan, and Yunnan. The eight mountain ranges stretch from the southern edge of the Himalayas in the south to the Kunlun Mountains, the Argin Mountains, and the northern edge of the Qilian Mountains in the north, the Pamir Plateau and the Karakoram Mountains in the west, and the western section of the Qinling Mountains and the Loess Plateau in the east and northeast (Figure 1).

Climatic conditions are typical of the plateau climate, and the climate at the eastern edge is distributed in gradient zones. The spatial distribution of precipitation is significantly different, it overall decreases from southeast to northwest, and the maximum annual average precipitation reaches more than 2000 mm. The temperature difference between day and night is large, the southern part of the southern Valley of Tibet is high, and the northern Tibetan plateau is low all year round. Due to its unique geographical location and extreme climatic conditions, most of the Tibetan Plateau is an alpine meadow, and permafrost is widely distributed [42]. The vegetation distribution is vertically zonal, distributing from south to north in forests, meadows, plateaus, grasslands, deserts, and semi-desert areas. The Tibetan Plateau, known as the "Water Tower of Asia" around the world, is widely distributed in rivers, lakes, and glaciers (among which the marine glacier water conservation capacity in Southern Tibet is extremely strong), which provide important support for the output and conservation of water resources in many places [43–45].

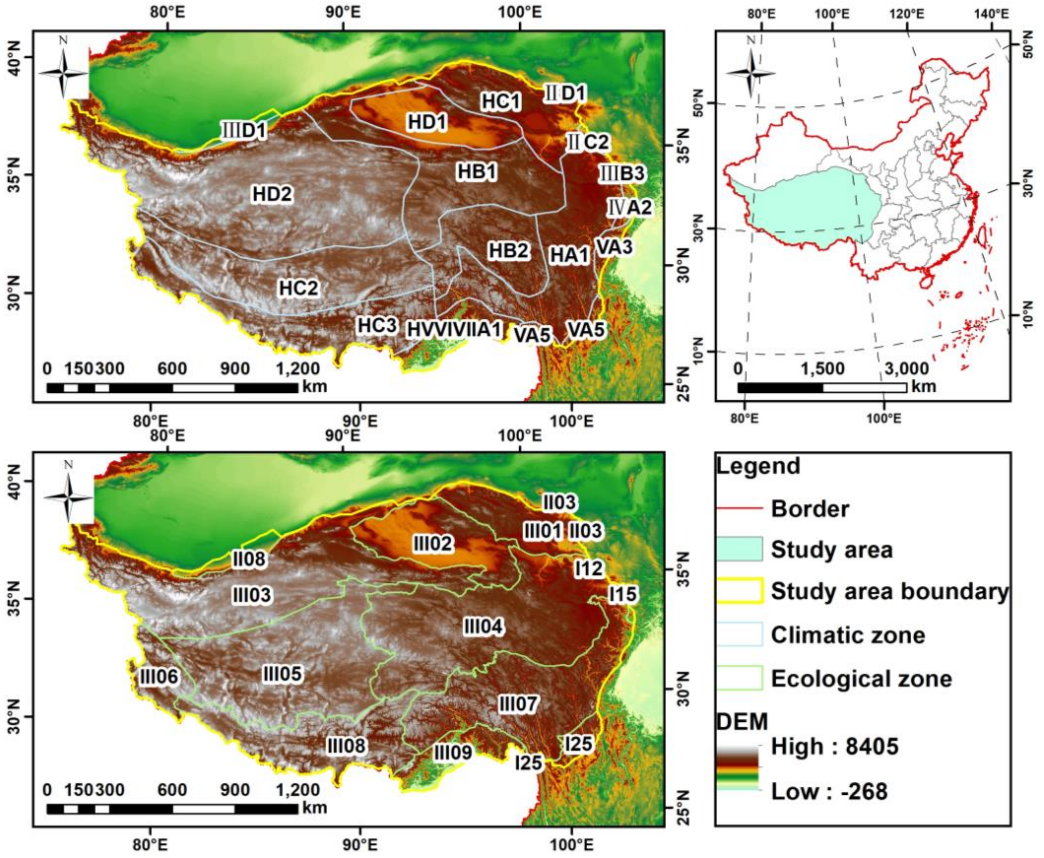

Figure 1. Geographical location and spatial distribution of elevation on the Tibetan Plateau; climatic regionalization is superimposed in the upper figure, and ecological regionalization is superimposed in the lower figure. Names and corresponding codes of each climate/ecological zone are shown in Tables 1 and 2, respectively.

Table 1. Names and corresponding codes of each climate zone.

First-Level Zone Code	First-Level Climate Zone	Second-Level Zone Code	Second-Level Climate Zone
II	Middle Temperate Zone	IIC2	Central Mongolia
		IID1	Menggan
III	South Temperate Zone	IIID1	Nanjiang
		IIIB3	Weihe
IV	North Subtropical Zone	IVA2	Qinba
V	Middle Subtropical Zone	VA3	Sichuan
		VA5	Northern Yunnan
H	Plateau Climate Zone	HD2	Northern Tibet
		HC3	Southern Tibet
		HC2	Central Tibet
		HB2	Changdu
		HA1	Bomi–Western Sichuan
		HVVIVIIA1	Dawang–Chayu
		HC1	Qilian–Qinghai Lake
		HB1	Southern Qinghai
		HD1	Qaidam

Table 2. Names and corresponding codes of each ecological zone.

Code	Ecological Zone
I12	Agricultural and grassland ecological area of the Loess Plateau
I15	Ecological area of deciduous and evergreen broad-leaved forest in Qinba Mountains
I25	Ecological area of evergreen broad-leaved forest in Southwest Sichuan and North Central Yunnan
II03	Grassland desertification ecological area in the middle of Inner Mongolia Plateau
II08	Tarim Basin–Eastern Xinjiang desert ecological area
III01	Qilian Mountain forest and alpine grassland ecological area
III02	Desert ecological area of Qaidam Basin
III03	Pamir–Kunlun–Altun alpine desert grassland ecological area
III04	River source area–Gannan alpine meadow grassland ecological area
III05	Alpine desert grassland ecological area of northern Tibetan Plateau
III06	Ali Mountain warm arid desert ecological area
III07	Cold temperate coniferous forest ecological area in Eastern Tibet–Western Sichuan
III08	Alpine meadow grassland ecological area in Southern Tibet
III09	Seasonal rainforest ecological area of tropical rain forest in Southeast Tibet

2.2. Data Sources and Data Processing

Based on the data requirements of the InVEST model water yield module and influencing factor analysis, long-term sequence data such as precipitation (P), reference evapotranspiration, DEM data, soil maximum root depth, land use type, primary watershed, and biophysical coefficients were collected from remote sensing products such as the Moderate-Resolution Imaging Spectroradiometer (MODIS) and converged datasets such as the TerraClimate dataset from Google Earth Engine (GEE) and so on. Specific data sources and descriptions are shown in Table 3, and the biophysical parameters of the water production module of the InVEST model are given in Table 4.

Table 3. Date sources and data descriptions.

Data Name	Date Source	Spatial Resolution	Data Description
Annual precipitation	Monthly climate and climate–water balance datasets on the global land surface, TerraClimate (https://www.nature.com/, accessed on 1 April 2023)	5 km × 5 km	Has relatively fine spatial resolution to fill gaps in climate data.
Average annual reference evapotranspiration	Monthly climate and climate–water balance datasets on the global land surface, TerraClimate (https://www.nature.com/, accessed on 1 April 2023)	5 km × 5 km	On the basis of the data, the water balance model is used to derive the monthly surface water balance dataset.
Average annual actual evapotranspiration	InVEST model	500 m × 500 m	Derived from the calculation results of the InVEST model water production module.
DEM data	Resources and Environmental Sciences and Data Center, Chinese Academy of Sciences (https://www.resdc.cn/, accessed on 1 April 2023)	500 m × 500 m	Radar topographic mapping SRTM derived from the U.S. Space Shuttle Endeavour.

Table 3. *Cont.*

Data Name	Date Source	Spatial Resolution	Data Description
Max root depth	Soil dataset of China at the World World Soil Database (HWSD) (v1.1) (2009) (http://poles.tpdc.ac.cn/, accessed on 1 April 2023)		It contains detailed data such as maximum soil root depth (mm), clay content (%), powder content (%), sand content (%), organic matter content (%), soil bulk density (g/cm^3), and so on.
Land use/land cover (LULC)	Terrestrial Process Distributed Activity Archiving Center (LP DAAC) MOD12Q1 (https://lpdaac.usgs.gov/, accessed on 1 April 2023)	500 m × 500 m	It was obtained by supervising classification processing by MODIS Terra and water reflectivity data, combining prior knowledge and supporting information.
NDVI	Terrestrial Process Distributed Activity Archiving Cente (LP DAAC) MOD13A1 v006 (https://lpdaac.usgs.gov/, accessed on 1 April 2023)	500 m × 500 m	Contains enhanced vegetation index (EVI), which improves sensitivity to areas of high biomass.
LAI	Terrestrial Process Distributed Activity Archiving Cente (LP DAAC) MOD15A2H v006 (https://lpdaac.usgs.gov/, accessed on 1 April 2023)	500 m × 500 m	A composite dataset of 8 days, combining LAI and photosynthetic effective radiation fraction (FPAR) products.
Primary watershed data	Resources and Environmental Sciences and Data Center, Chinese Academy of Sciences (https://www.resdc.cn/, accessed on 1 April 2023)	(Vector data)	It includes all river networks in the country and all sub-basins with an area greater than 100 km^2.
Biophysical coefficients	Refer to the existing literature [46]		Includes the type coefficient, maximum root depth, and evapotranspiration coefficient Kc for each type of land use type.
Zhang parameter (Z)	Refer to the existing literature [46]	(Empirical onstant)	It is a seasonal factor that can capture precipitation patterns and other hydrogeological features in the study area, and set Z = 15.
Climate zone data	Resources and Environmental Sciences and Data Center, Chinese Academy of Sciences (https://www.resdc.cn/, accessed on 1 April 2023)	(Vector data)	This dataset is a map of China's climate zoning compiled by the National Meteorological Administration of China in 1978, using climate data from 1951 to 1970.
Ecological zone data	Ecosystem Assessment and Ecological Security Database in China (http://www.ecosystem.csdb.cn/, accessed on 1 April 2023)	(Vector data)	On the basis of ecological regions, ecological zones and ecological sub-regions are divided.

Table 4. Biophysical parameters of water production module of InVEST model.

Land Use Type Code	Name of Land Use Type	Land Use Type Coefficient	Max Root Depth (mm)	Transpiration Coefficient Kc
1	Evergreen coniferous forest	1	5000	0.9
2	Broad-leaved evergreen forest	1	5000	0.9
3	Deciduous coniferous forest	1	5000	0.9
4	Deciduous broad-leaved forest	1	5000	0.9
5	Mixed forest	1	5000	0.9
6	Enclosed bush	1	5000	0.9
7	Open shrub	1	5000	0.9
8	Woody savanna	1	600	0.65
9	Savanna	1	600	0.65
10	Grassland	1	600	0.65
11	Permanent wetland	0	1	1
12	Cultivated land	1	500	0.65
13	Urban and built-up land	0	1	0.3
14	Farmland/natural vegetation	1	500	0.65
15	Permanent ice and snow	0	1	1
16	Poor land	0	1	0.3
17	Body of water	0	1	1

2.3. Methodology

The Integrated Valuation of Ecosystem Services and Trade-offs (InVEST) model can simulate the change in the quality and value of ecosystem services systems under different land cover scenarios, and realize the spatialization and visualization of the quantitative assessment of the ecosystem services' functional value. The water yield estimation module in the InVEST model calculates the water yield based on the principle of water balance via parameters such as precipitation, surface evaporation, vegetation transpiration, soil depth, and root depth [47,48]. This model is used to calculate the multi-year water yield of the Tibetan Plateau, and to analyze and explore the spatiotemporal evolution of the water yield capacity of the Tibetan Plateau and its regularities. The flowchart of the study is shown as Figure 2. Based on the 500 m scale, this study conducts a long-sequence assessment of the water yield on the Tibetan Plateau over many years, using the Budyko hydrothermal coupling equilibrium hypothesis, and the formula is as follows:

$$Y_{xi} = \left(1 - \frac{AET_{xi}}{P_x}\right) \times P_x \tag{1}$$

where Y_{xi} is the annual water yield of grid cell x on land use type i; P_x is the total annual precipitation on grid x; AET_{xi} is the annual actual evapotranspiration of land use type i on raster x. Calculations are based on the improved method of [7] as follows:

$$\frac{AET_x}{P_x} = \frac{1 + w_x R_{xj}}{1 + w_x R_{xj} + \left(\frac{1}{R_{xj}}\right)} \tag{2}$$

where R_{xi} is the dryness index (dimensionless) of grid cell x on land use type i, obtained by the ratio of the potential evapotranspiration to the precipitation. w_x is an empirical parameter representing a non-physical parameter of climate and soil properties [30] and is the ratio of the modified annual PAWC to expected precipitation. The specific function formula of w_x is as follows:

$$w_x = Z \times \frac{AWC_x}{P_x} \tag{3}$$

where w_x represents the linear function $AWC_x \times N_p$, N is the number of rainfall events per year, AWC_x represents the available water content of plants, and Z represents the hydrogeological features and seasonal distribution of precipitation.

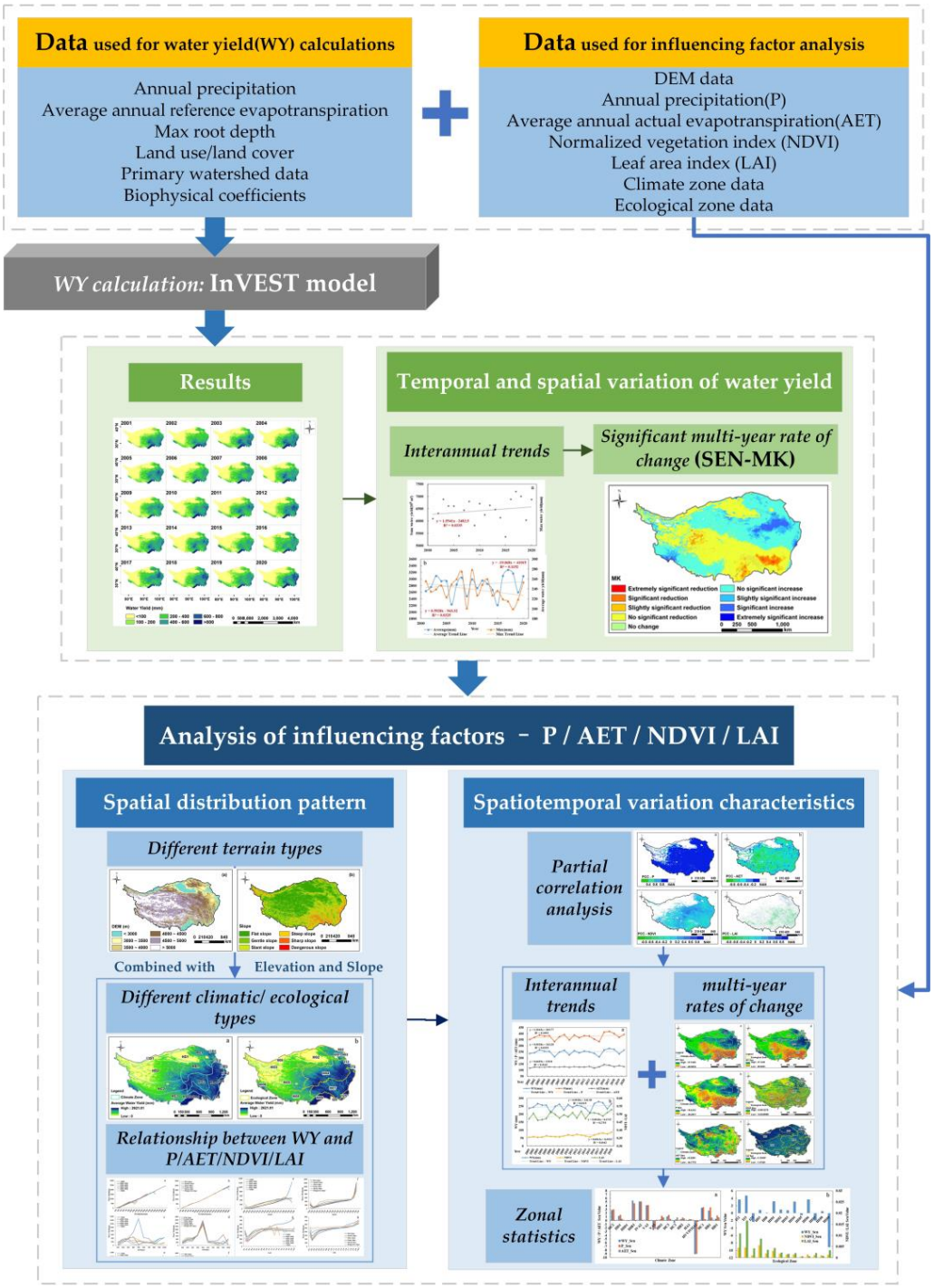

Figure 2. The flowchart of the study.

The principle of PAWC refers to the existing literature [28,48], and it is used to calculate the difference between the amount of water held in the field and the permanent wilt coefficient. The formula is as follows:

$$\mathrm{FMC} = 0.003\,075 \times \mathrm{Sand} + 0.005\,886 \times \mathrm{Slit} + 0.008\,039 \times \mathrm{Clay} + 0.002\,208 \times \mathrm{OM} - 0.143\,40 \times \mathrm{BD} \quad (4)$$

$$\mathrm{WC} = -0.000\,059 \times \mathrm{Sand} + 0.001\,142 \times \mathrm{Silt} + 0.005\,766 \times \mathrm{Clay} + 0.002\,228 \times \mathrm{OM} + 0.026\,71 \times \mathrm{BD} \quad (5)$$

where FMC is the field water holding capacity (%), WC is the permanent wilt coefficient, Clay is the soil clay particle content (%), Silt is the soil silt content (%), Sand is the soil sand content (%), OM is the soil organic matter content (%), and BD is the soil bulk density (g/cm^3).

3. Results

3.1. Water Yield Calculation Results and Verification

Based on the InVEST model's water yield module, the water yield of the Tibetan Plateau for a long-term series was calculated, and the results are as shown in Figure 3. The results are verified by using the water resource statistics of the Tibetan Plateau (2004–2016) as the true values, and the datasets include the water resource statistics of Tibet and Qinghai, which originated from the Tibet Water Resources Bulletin and the Qinghai Water Resources Bulletin, and are the statistical scales of the municipal units. The data of 2004, 2008, 2012, and 2016 are selected for accuracy testing, and the results of Table 5 show that the simulation accuracy of the water yield is good, with an average relative error of 7.47% and a maximum relative error of no more than 11.08%.

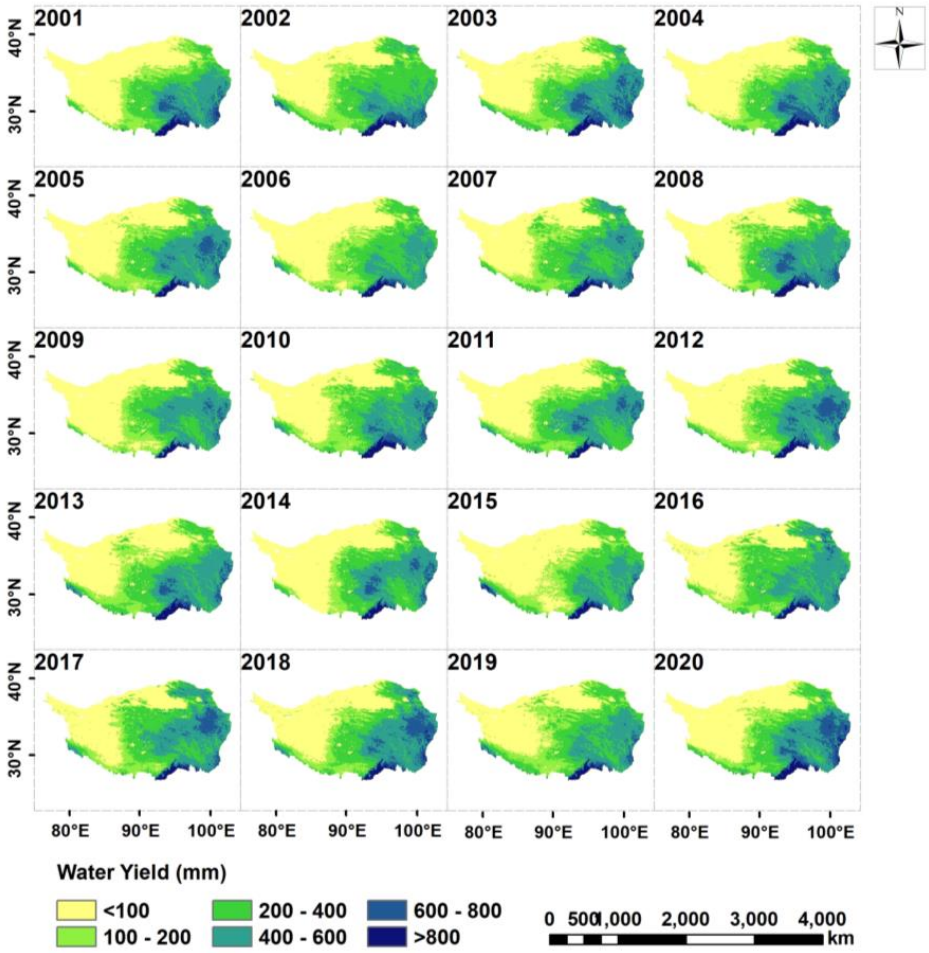

Figure 3. Calculation results of water production based on InVEST model.

Table 5. Comparison and accuracy test of water yield measurement value with true value.

Year	Measurements (10^8 m^3)	True Value (10^8 m^3)	Relative Error
2004	4777.727	5373.002	11.08%
2008	5076.571	5313.416	4.46%
2012	4748.039	5182.336	8.38%
2016	5035.244	5354.324	5.96%

In the past 20 years, the overall spatial distribution pattern of the water yield on the Tibetan Plateau has been consistent, showing a decreasing trend from southeast to northwest. The total annual water yield is 12,840.31 km^3, the average annual total water yield is 642.02 km^3, and the total annual water yield is the highest at 718.99 km^3 and the lowest at 535.78 km^3, confirming that this is a high-water-yield area.

The degradation of the permafrost and the thickening of the active layer will inevitably lead to the conversion of a large amount of underground ice in the permafrost into liquid water [49,50]. Moreover, as the permafrost is no longer frozen after degradation, the permeability coefficient of the original frozen aquifer will suddenly increase and form a runoff channel, resulting in an increase in river recharge and an increase in river runoff [51]. Since the InVEST model water yield module does not consider the impact of plateau frozen soil degradation on water resources, the results of this study tend to be underestimated. The study of water resources considering the degradation of permafrost on the Qinghai–Tibet Plateau is worthy of further consideration.

3.2. Temporal and Spatial Variation in Water Yield

In the past 20 years, there have been large differences in the interannual variation in the water yield of the Tibetan Plateau, but the overall trend of a slow rise is shown. The time change trend was analyzed at five-year intervals, and it can be seen that the water yield in the first two years showed a significant growth trend, while the last two years have a clear downward trend, but the water yield capacity has been slightly enhanced in the past five years. From Figure 4a, it is seen that the total annual water production ranges from 5357.77 to 7189.95 billion m^3, and the average annual total water production from 2001 to 2020 is 6420.15 billion m^3. From Figure 4b, it is seen that the average water yield is 200–280 mm and shows a slow upward trend; the maximum value is 2100–3300 mm, which shows a clear downward trend. It is inferred that due to natural and man-made factors, the overall water yield in this area has gradually increased, while the extreme-water-yield areas have been regulated and improved. Using the Sen-MK trend analysis method, as shown in Figure 5, it was found that the overall multi-year water yield has experienced an increase–decrease–increase trend from northeast to southwest, and the areas with significant increases and significant decreases are mainly symmetrically distributed in the east, while a small number of significantly increased areas are concentrated in the southwest marginal area. The areas with no change in water yield are scattered in the northwest corner, where is no water yield all year round. The areas with an increasing water yield accounted for 31.96% of the total area, and the areas with decreasing values accounted for 15.40%.

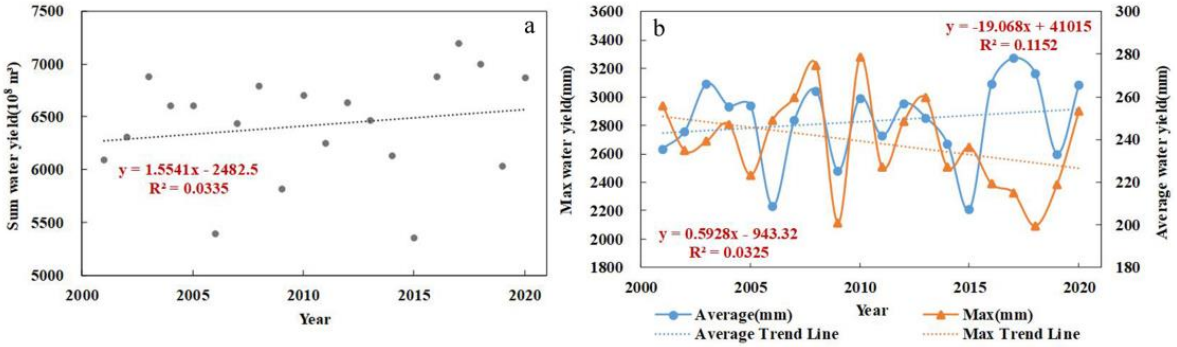

Figure 4. The total WY in the study area in the past 20 years (**a**); trend of average and maximum annual WY in the study area (**b**).

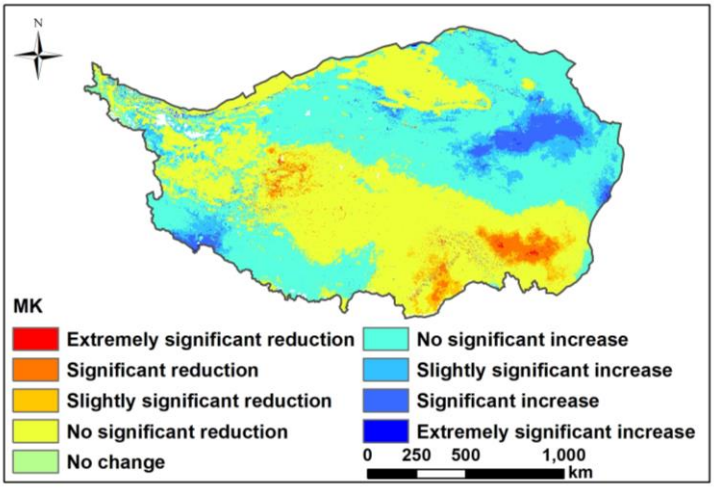

Figure 5. Sen-MK test results of annual WY in the study area.

4. Discussion

The Tibetan Plateau has a strong water conservation capacity and is known worldwide as the "Asian Water Tower", providing a steady stream of water resources for Asia and even the world, and it is also a powerful regulator of the water resource cycle. The geographical conditions are unique in the study area: the climatic conditions are extreme and changeable all year round, and the ecosystem is extremely sensitive, which has an important impact on the spatial distribution pattern of the water yield and the characteristics of spatiotemporal changes in the area. Moreover, to a certain extent, it also determines the water yield capacity and water conservation capacity of the region [52]. In order to explore the influencing factors of the spatial distribution pattern and spatiotemporal variation characteristics of the water yield capacity on the Tibetan Plateau, this paper explores the differences in the spatial distribution patterns of the water yield from the perspective of different terrain types, climate types, and ecological types, selecting four factors with an important influence on P, AET, NDVI, and LAI, exploring the effects and influence laws of climate change and vegetation change on the spatiotemporal variation characteristics of the water yield under different climate types and ecological types [53–55].

4.1. Analysis of Influencing Factors of Spatial Distribution Pattern

4.1.1. Spatial Distribution Pattern of Water Yield under Different Terrain Types

Figure 6 shows that the water yield in the eastern part of the Tibetan Plateau is significantly higher. The altitude of this area is low; it belongs to the Sanjiangyuan Area and the valley of the upper reaches of the Brahmaputra River and other rivers, and there are many local plains along the valleys. The southernmost part of the region has a very high water yield capacity, which is closely related to the distribution of its oceanic glaciers and its low-altitude characteristics. The water yield in the large areas of the north and west tends to be zero all year round, and the northern Qaidam Basin displays the plateau's continental climate, with drastic temperature changes, mainly characterized by droughts. A series of high-altitude mountains are distributed in the west, with snowy peaks and widespread glaciers all year round, resulting in an extremely weak water yield capacity.

Based on the above characteristics of the water yield, the spatial distribution pattern of the water yield on the Tibetan Plateau under different elevations and slopes was explored from the perspective of topography. The general correlation between elevation, slope, and water yield was −0.31 and 0.37, respectively. The elevation and water yield were weakly negatively correlated, and the slope and water yield were weakly positive. The elevation is divided into six categories: <3000 m, 3000~5000 m, 3500~4000 m, 4000~4500 m, 4500~5000 m, and >5000 m. The slope is also divided into six categories: flat slope (0~5°), gentle slope (5~8°), steep slope (15~25°), sharp slope (25~35°), and dangerous

slope (>35°) [56]. The results show that the overall elevation of the study area increases from east to west, and the central and western areas are large in the high-altitude area of more than 4500 m, while the eastern altitude is mostly 4000–4500 m and less than 3000 m. Moreover, the study area is mostly of a flat slope, followed by a slant slope, and the southeast slope is steep, mainly due to the distribution of the important Hengduan Mountain Range in China. Statistics on the area proportion of various altitudes and slopes and the average water yield of the pixel scale are shown in Figure 3. The water yield at the pixel scale shows a downward trend with the increase in altitude and an increasing trend with the increase in slope, in which the water yield at 3000–4000 m above sea level increases significantly with the increase in altitude.

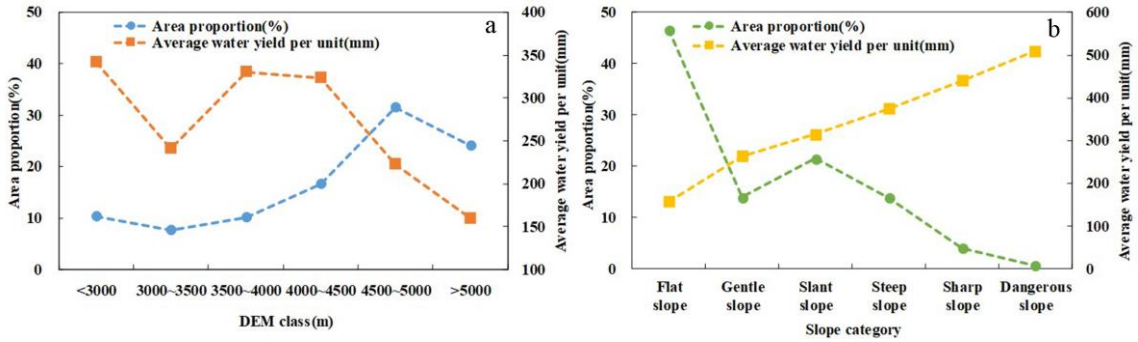

Figure 6. Water yield per unit of magnitude (**a**) and slope (**b**).

4.1.2. Spatial Distribution Patterns of Water Yield under Different Climatic Types

Based on climate zones, the influence of different climate types on the spatial layout of WY is explored. As shown in Figure 7a, it can be seen that the plateau climate in the study area is widely distributed (accounting for 96.75% of the total area), and the eastern marginal climate zone shows a gradient distribution, from high latitude to low latitude, which is in the middle temperate zone, the southern temperate zone, the northern subtropical zone, and the central subtropical zone; a small part of the northwest edge is in the southern temperate zone. Statistics of the total value, mean value, and standard deviation of WY in each region show that the highest WY is found in the plateau climate zone, but due to the comprehensive influence of various factors, such as the topography and landform, the average value of WY is low and the distribution is extremely unstable. The mean WY in the central and northern subtropical regions is high and relatively stable. Statistics of the WY per unit area (mm/km^2) of each climate zone are shown in Figure 8a, and it is found that the plateau climate zone has a vast area but extremely low WY capacity. The central subtropical and northern subtropical WY is high, with strong WY capacity and water conservation potential.

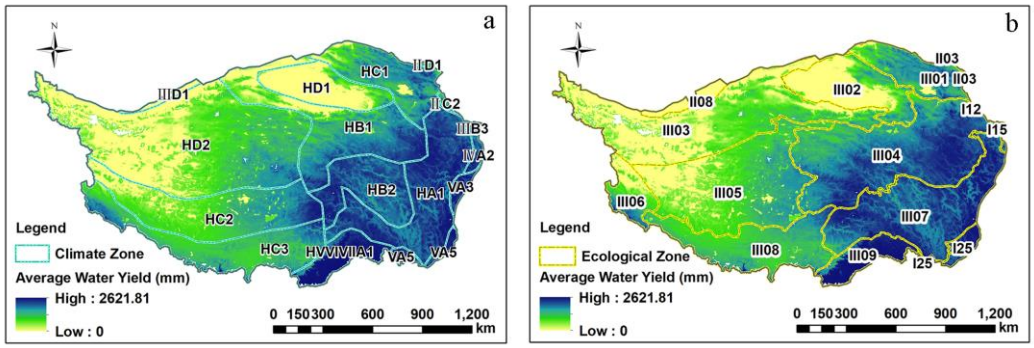

Figure 7. Spatial distribution of water production in different climate zones (**a**); spatial distribution of water production in different ecological zones (**b**).

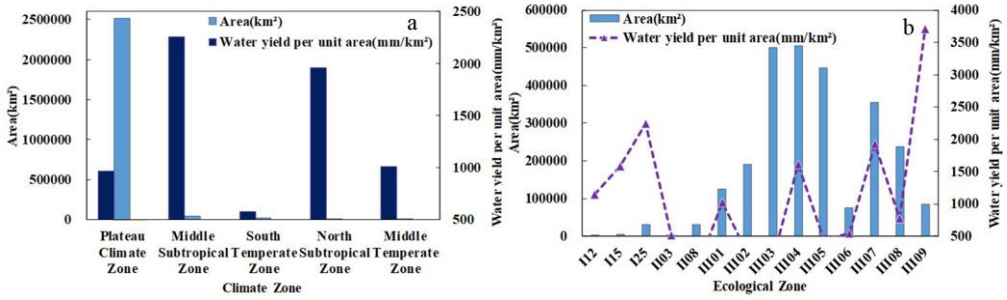

Figure 8. Water yield per unit area in each climate zone (mm/km^2) (**a**); water yield per unit area in each ecological zone (mm/km^2) (**b**).

The impact of climate change on WY is complex and profound. P and AET are selected as climate impact factors, and the topographic features are combined to analyze them. As seen in Figure 9a,b, under different elevation and slope categories, the WY increases linearly with the increase in P, and the positive impact of P on WY is speculated to be less constrained by the terrain. Among them, the higher the altitude, the less the WY data, which indirectly confirms the negative correlation between altitude and WY. As seen in Figure 9c, under different elevation categories, the relationship between AET and WY is mainly of two types. At altitude ≥3000 m, the WY does not change notably with the increase in AET, and the average WY is approximately 200 mm. When the altitude is below 3000 m, the WY shows an increase (AET = 0~500 mm) and a sharp drop (AET = 500~800 mm) with the increase in AET. As seen in Figure 9d, under different slope types, the WY of each slope showed a consistent upward trend when AET < 500 mm, the WY decreased consistently when AET = 500–600 mm, and the relationship between the three showed different changes when AET > 600 mm. On the whole, when the altitude is below 3000 m and the slope is gentle, steep, or sharp, the effect of AET on WY is essentially the same. The change from rising to falling occurs at AET = 500 mm, and the rebound phenomenon occurs after the AET value increases to a certain extent. In summary, it is speculated that before AET = 500 mm, the P is the dominant driving force on the WY function, the negative force of AET at AET = 500~600 mm is gradually greater than that of P, and there is a slight rebound in WY after AET ≥ 500 mm.

4.1.3. Spatial Distribution Patterns of Water Yield under Different Ecological Types

The spatial distribution pattern of WY in different regions is explored, and the WY capacity per unit area in different types of ecological zones is explored. From Figure 7b, it can be seen that the ecological areas with the largest coverage are III03, III04, III05, and III07. Statistics of the total value, mean value, and standard deviation of WY in each ecological region are shown in Figure 6; it can be seen that the distribution stability of WY has obvious regional heterogeneity, and the overall situation is gradually stable from south to north, and east to west. The most stable ecological areas are the III06 Alishan Temperate Arid Desert Ecological Zone and the III09 Southeast Tibet Tropical Rainforest Monsoon Rainforest Ecological Zone, the former due to the annual small amount of WY and the latter due to the annual abundance of WY. The unit area WY (mm/km^2) of each ecological region was calculated, and the ecological regions with low unit WY capacity were found in the north (Figure 8b), namely II03, II08, III02, III03, III05, and III06. The ecoregions with higher unit WY capacity are distributed in the southeast, namely III09, I25, and III07, and have high WY capacity and water conservation potential. Among them, III03, III04, III05, and III07, which are widely distributed, have low WY values. For III09, due to the comprehensive influence of the tropical rainforest climate and natural conditions of oceanic glacier distribution, the total WY value is in the middle, the mean value and stability are high, and the WY capacity cannot be ignored.

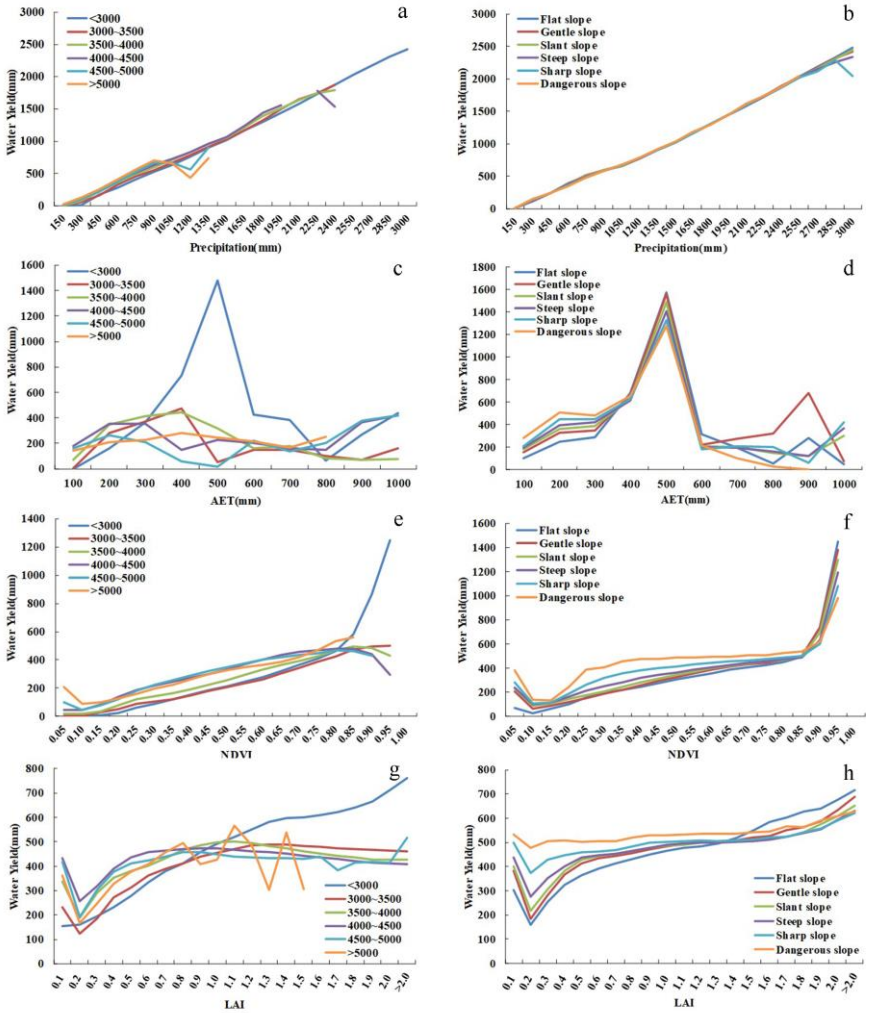

Figure 9. Relationship between P/AET/NDVI/LAI and WY at different altitudes and slopes. Relationship between P and WY at different altitudes (**a**) and slopes (**b**); Relationship between AET and WY at different altitudes (**c**) and slopes (**d**); Relationship between NDVI and WY at different altitudes (**e**) and slopes (**f**); Relationship between LAI and WY at different altitudes (**g**) and slopes (**h**).

Combining vegetation factors and topographic factors, the spatiotemporal variation characteristics of WY on the Tibetan Plateau were analyzed. As seen in Figure 9e,f, at different altitudes and slopes, the relationship between NDVI and WY showed a linear growth trend. The WY at NDVI < 0.01 decreased significantly, and the WY at 0.01< NDVI < 0.90 gradually increased. When the NDVI > 0.90, the WY in areas with an altitude of less than 3000 m and all types of slopes surged, and it is speculated that when the vegetation coverage is extremely high, the high altitude has a negative effect on the WY, and the slope type will not affect the WY capacity. As seen in Figure 9g,h, for different altitude and slope types, when LAI < 0.2, the WY decreases with the increase in LAI; however, when the altitude is less than 3000 m, the WY increases almost linearly with the increase in LAI. It can be concluded that an increasing LAI at low altitudes of less than 3000 m will help to enhance the WY function, and with a larger LAI at 3000 m and above, the WY is not necessarily higher. When LAI > 0.2, the WY in the area of 3000–5000 m increases to different values and decreases slowly; however, when the altitude is greater than 5000 m, the WY fluctuates after LAI > 0.8. When LAI > 0.2, the WY at each slope increases to varying degrees with the increase in LAI, and the lower the slope, the higher the WY but the lower the growth rate.

4.2. Analysis of Influencing Factors of Spatiotemporal Variation Characteristics

Based on the above characteristics of water yield change, the effects of changes in climate factors and vegetation factors on the spatiotemporal variation characteristics of the water yield were further explored in this study. Ebrahim Ghaderpour et al. proposed a more advanced coherence and phase delay analysis method, helping to understand uncertainty analysis in MODIS. Specifically, the least-squares wavelet software and Pearson correlation coefficient were used to analyze the consistency and phase delay between land cover and climate [57]. It is speculated that there is a high probability of correlation and phase delay between the climate, vegetation, and water yield; meanwhile, the selection of correlation analysis methods suitable for the characteristics of the data themselves will greatly improve the accuracy and scientificity of the results. Since (i) the climate and vegetation data used in the study may have outliers and do not show a normal distribution, and (ii) there is a phase delay between the data, it is more appropriate to explore the monotonic relationship (Spearman-based correlation analysis) than the linear relationship (Pearson-based correlation analysis). Thus, this study uses Spearman-based partial correlation analysis. This method has no requirement for a normal distribution of data and is not sensitive to data errors and extreme values, making it more suitable for correlation analysis related to climate data. For the Spearman correlation analysis of long-time-series data, this used the MATLAB software to obtain the spatiotemporal variation characteristics of the correlation coefficient (Figure 10). The specific analysis is as follows.

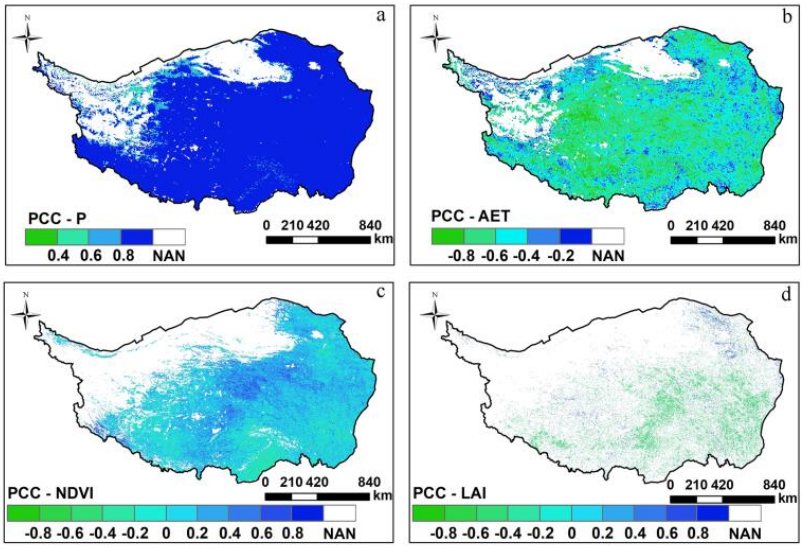

Figure 10. Distribution of partial correlation coefficient between WY and P/AET/NDVI/LAI (**a**–**d**).

4.2.1. Analysis of the Influencing Factors of Climate Change on the Spatiotemporal Changes in Water Yield

Due to the unique geographical location, topography, and plateau climate of the Tibetan Plateau, it has become a very sensitive area affected by global changes, and it is regarded as a "climate change laboratory" by China; with the recent global changes, the Tibetan Plateau has shown a warming trend [58]. The simple correlations between P, AET, and WY in the study area were calculated as 0.98 and 0.56, respectively. P and WY showed a strong positive correlation, while AET and WY showed a moderate positive correlation. In order to exclude the influence of the two on their respective correlations, the degree of correlation was calculated using the partial correlation analysis method based on the Spearman method, and Figure 10a,b show the spatial distribution of the partial correlation coefficients of P and AET on WY. The P and WY partial correlation coefficients (PCC) that passed the *t* test were 0.40~1.00 (average PCC = 0.96 on the cell scale). P and WY were strongly positively correlated, of which the significant positive correlation region accounted for 97.26% of the effective area, and P and its spatiotemporal distribution gave a

positive response to WY. The PCC of AET and WY that passed the *t* test was −1~0 (average PCC = −0.57 on the cell scale). AET and WY showed a moderate negative correlation, of which the significant negative correlation region accounted for 49.63% of the effective area. AET and its spatiotemporal distribution exert different degrees of inhibition on the water yield function. Meanwhile, the partial correlation results show that the P factor is able to enhance the positive correlation of AET and WY to some extent.

Based on the correlation between P, AET, and WY, the interannual change trend of the three from 2001 to 2020 was explored. As shown in Figure 11a, it can be seen that P, AET, and WY have shown a slow upward trend in the past 20 years, the overall change trend of P and WY is consistent, and the AET change tends to be stable. Based on different climate types, as shown in Figure 12a,b, the spatial distribution of the P and WY change rate is consistent in that the increase trend is seen in the northeast, the decrease trend is seen in the south, and the trends in the north and west have not changed. The areas with significant increases or decreases are mainly concentrated in the eastern region, and the overall rate of change of AET is decreasing from east to west (Figure 12c). In general, the rate of change of P has a positive effect on the rate of change of WY, and the rate of change of AET has a negative impact on the rate of change of WY, while the change in P dominates the water yield capacity. According to the statistics of the change rates of the three climate zones in Figure 13a, it can be seen that the change rate of the water yield in each climate zone is essentially dominated by the change rate of P, and the AET in the plateau climate zone is higher and has a significant negative impact.

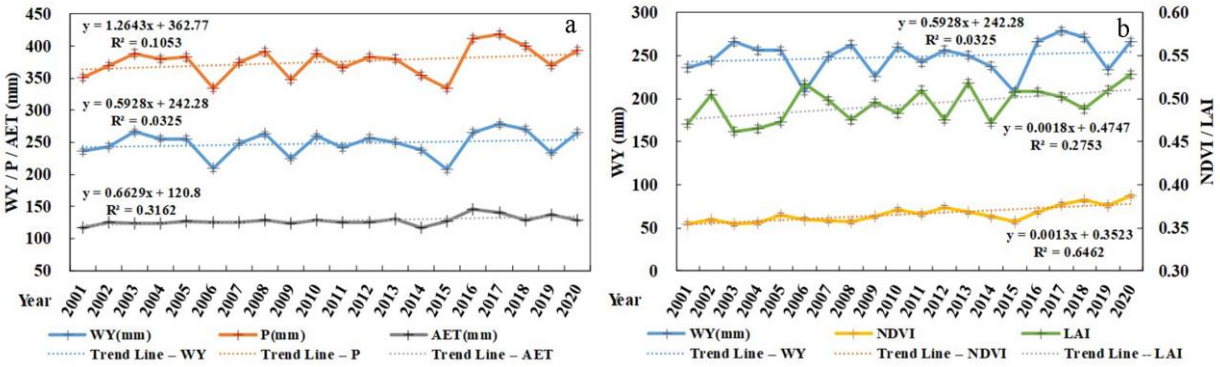

Figure 11. Spatial distribution of WY, P, and Sen change rate in different climate zones (2001–2020) (**a**); spatial distribution of WY, NDVI, and LAI Sen change rate in different climate zones (2001–2020) (**b**).

4.2.2. Analysis of the Influencing Factors of Vegetation Change on the Spatiotemporal Changes in Water Yield

As one of the most important components of terrestrial ecosystems, vegetation participates in and regulates the circulation of natural matter and energy, and its spatiotemporal distribution and change profoundly affect the evolution of water resource ecosystems [59,60], among which the common vegetation remote sensing monitoring parameters are NDVI and LAI. The simple correlations between NDVI, LAI, and WY in the study area were calculated to be 0.74 and 0.49, respectively. NDVI showed a moderate positive correlation with WY, and LAI showed a weak positive correlation with WY. Figure 10c,d show the spatial distribution of the PCC of NDVI and LAI on WY. The PCC of WY and NDVI that passed the *t* test is −0.82~0.93 (average PCC = 0.13 on the pixel scale), and it can be seen that NDVI and WY are weakly correlated, and the weak positive correlation region and the weak negative correlation area account for 18.48% and 47.75% of the effective area, respectively. The effect of NDVI and its spatiotemporal distribution on WY is extremely small. The PCC of WY and LAI that passed the *t* test is −0.90~0.92 (average PCC = −0.31 on the cell scale), which shows that LAI and WY are moderately negatively correlated, and the negative correlation area accounts for 97.87% of the effective area, while LAI and its spatiotemporal distribution mainly have a weak inhibitory effect on the water yield

function. In addition, it was found that NDVI and LAI can enhance the positive correlation of WY.

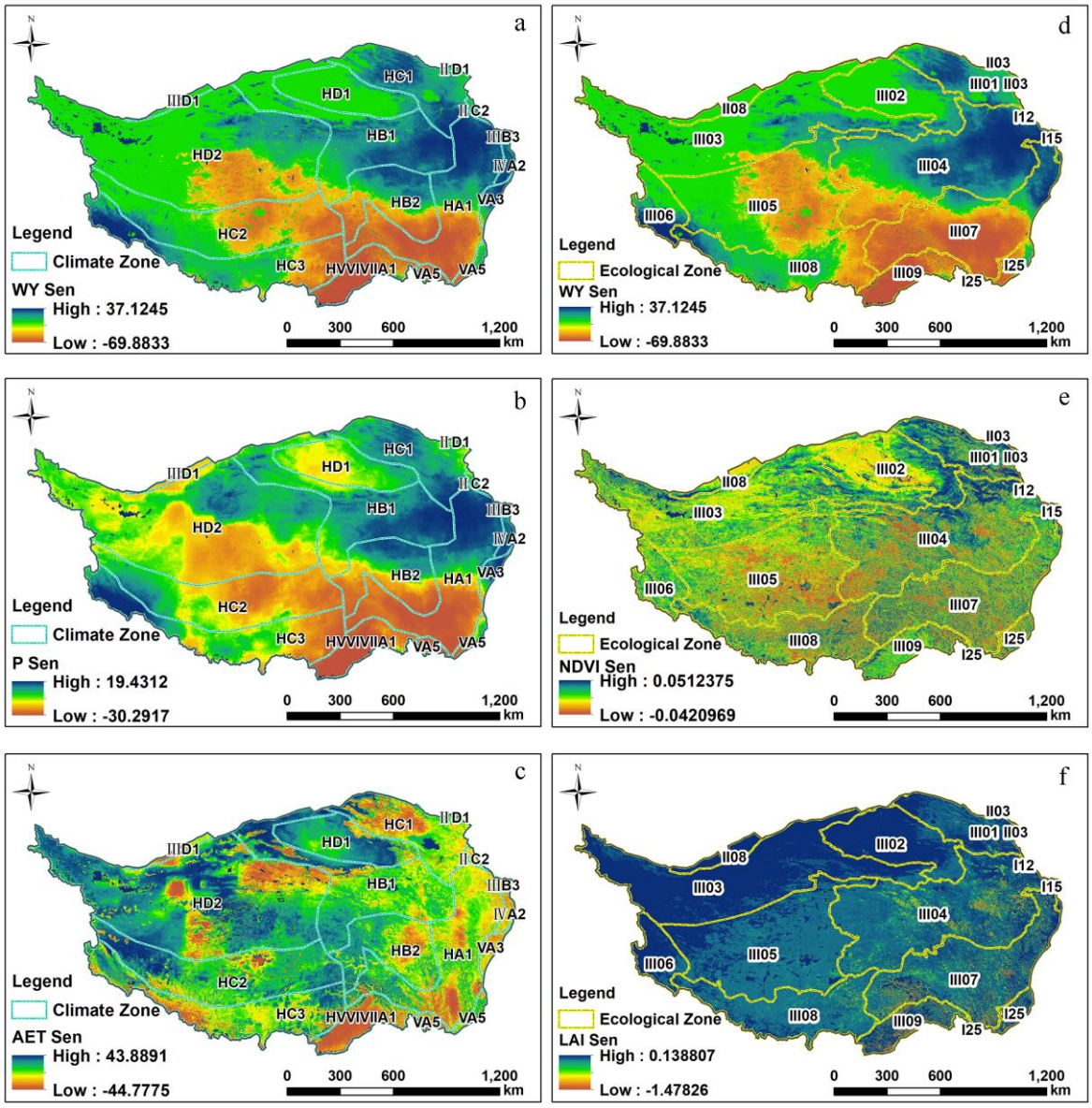

Figure 12. Interannual variation in average annual WY (**a**), P (**b**), and AET (**c**) under climatic zones; interannual variation in average annual WY (**d**), NDVI (**e**), and LAI (**f**) under ecological zones.

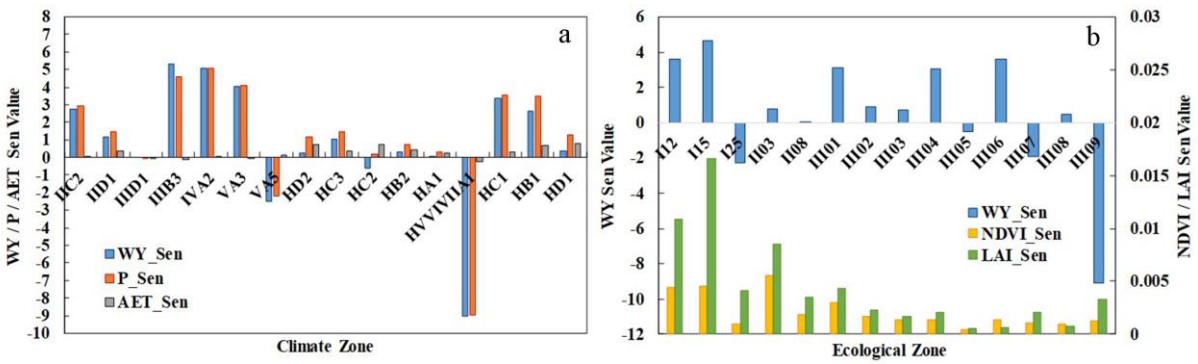

Figure 13. The rate of change of WY, P, AET under different climate zones (**a**); the rate of change of WY, NDVI, LAI under different ecological zones (**b**).

Based on this, in Figure 11b, it can be seen that NDVI, LAI, and WY have shown a slow upward trend in the past 20 years, the overall change trends of LAI and WY have similarities but the change trend is small, and the overall change in NDVI tends to be flat. After superimposing the ecological zones, as shown in Figure 12d,e, the spatial distribution of the change rate of NDVI and WY is almost inconsistent; only in the northeast is there an increasing trend, while the spatial distribution of the change rate of LAI and WY is not consistent (Figure 12f). The ecoregion with the widest positive correlation coverage area of NDVI is III04, which indirectly indicates that the meadow grassland vegetation cover in this area is better, and the water yield capacity and water conservation capacity are high. The negative correlation area was mainly concentrated in III09, and it is speculated that the weakening of the water yield capacity is due to different vegetation types. The weak positive correlation of LAI and WY covers a large proportion of the study area. It is found that regulating the NDVI will improve the water yield capacity and water conservation capacity, but its positive effect is weak due to the unique natural conditions. The statistics of the rate of change of the three under each climate zone are shown in Figure 13b, and it is found that the LAI growth rate is generally greater than that of the NDVI. The areas with large growth rates of NDVI, LAI, and WY were I12 and I15, both of which are distributed in the northeast border area, covering a small area. The growth rates of NDVI and LAI are high in the II03 region, but the WY growth rate is low due to the natural environment, such as the desert. There is no obvious regularity in the rate of change of the three in the III02-III09 region. It can be inferred that NDVI and LAI have little effect on the water yield function, but both of them can play a relatively obvious positive role in areas with a good ecological environment.

4.3. Uncertainty and Limitations

The adaptability of remote sensing product data to the Qinghai–Tibet Plateau is the main reason for the uncertainty and limitations of the results. In this regard, the main discussion is focused on the MODIS NDVI and TerraClimate data.

At present, the assessment of vegetation coverage and changes on the Qinghai–Tibet Plateau is mostly based on the NDVI [53,61–70], which is used as a representative of vegetation greenness and vegetation difference in hillside-scale research [61,71]. Since the Qinghai–Tibet Plateau is a typical complex mountainous terrain with obvious differences, the vegetation cover is greatly affected by the light conditions—for example, vegetation is greener on shaded slopes than on sunny slopes, and even has seasonal variations [71]. It is meaningful to compare indices such as the NDVI and EVI. The NDVI enables us to eliminate the terrain lighting effect: the NDVI is less susceptible to light conditions so that the effects can be even negligible [72]. The EVI is more sensitive to the terrain: the EVI overcomes saturation, but is strongly affected by the lighting conditions and the influence of shadows is more difficult to correct [73]; thus, it can be said to be more sensitive to the terrain conditions than the NDVI [72]. The spatial scale reduces the terrain effect: the terrain effect is related to the spatial scale, and the larger the pixel unit, the smaller the negative impact of the terrain on the NDVI, or it may even be negligible [72]. Moreover, the MODIS NDVI has advantages over the VHRR NDVI and SPOT VGT NDVI in terms of spatiotemporal resolution, spectral resolution, chlorophyll sensitivity, and the exclusion of water vapor interference; it is expected to be used for the dynamic monitoring of vegetation [62]. The AVHRR NDVI has a lower spatial resolution (1.1 km), while the Landsat NDVI (30 m) and Sentinel (−2) NDVI (up to 10 m) have a higher spatial resolution, but, due to the large study area, the MODIS NDVI was finally chosen. However, using MAIAC BRDF corrected products over MODIS will be meaningful for further research.

Datasets such as TerraClimate, with a high spatial resolution, were used in this study, which can better simulate the complex areas of the underlying surface and improve the spatial realism [74,75]. However, due to the lack of ground truth data/stations for calibration and verification in mountainous areas around the world, the real situation reflection capacity in and around the mountains of the Qinghai–Tibet Plateau is limited.

Therefore, for areas with complex terrain, such as the Qinghai–Tibet Plateau, to improve the accuracy and authenticity of the research results and promote the progress of research ideas, methods, and technologies, high-precision development and localization selection of product data are necessary and of great significance.

5. Conclusions

Based on the InVEST model, the water yield of the Tibetan Plateau in the past 20 years was obtained, and a comprehensive analysis of the influencing factors of the spatial distribution and spatiotemporal variation characteristics of the water yield was carried out from the three aspects of topography, climate, and ecology (vegetation), which provides theoretical support for the ecological environment governance and protection of the water yield function and water conservation on the Tibetan Plateau. The main findings of this paper are as follows:

(1) The total water yield of the Tibetan Plateau from 2001 to 2020 is 12,840.31 km^3, and it belongs to the high-water-yield area and has a strong water yield capacity. The spatial distribution of the water yield as a whole showed a decreasing trend from southeast to northwest, and the interannual variation was large but showed an overall slow increase.

(2) The water yield capacity is higher in the areas of less than 3000 m and 3500~4500 m above sea level. Moreover, the larger the slope, the stronger the water yield capacity. The plateau climate zone covers a wide range but has a low water yield capacity, and the central and northern subtropical water yield capacity is extremely strong. Ecoregions with a high water yield capacity are mostly covered with woodland and alpine meadows (III09, I25, III07).

(3) When the altitude is lower within a certain range, the precipitation tends to increase. The precipitation is the dominant factor in the water yield function when the AET < 500 mm, and the negative force of AET increases significantly when AET = 500~600 mm, gradually offsetting the precipitation effect.

(4) When the vegetation coverage is extremely high, the high altitude has an inhibitory effect on the water yield. The water yield at an altitude of less than 3000 m has an almost linear growth relationship with LAI. The water yield decreases with the increase in LAI when LAI < 0.2, while the water yield at various slopes increases at different rates with the increase in LAI when LAI > 0.2. Moreover, the lower the slope, the higher the water yield and the lower the growth rate.

(5) The spatial distribution of the change in precipitation and water yield is consistent, both showing an increase–decrease–increase trend from northeast to southwest, and there is a significant positive correlation. The areas with significant increases and decreases are concentrated in the east and are symmetrically distributed upwards and downwards. Precipitation and NDVI changes have a positive effect on changes in water yield, while changes in AET and LAI have a negative effect on changes in water yield.

Author Contributions: Conceptualization, L.L., H.S. and L.H.; formal analysis, L.L., L.H. and X.W.; funding acquisition, H.S., L.L. and X.W.; investigation, L.L., L.H., X.W. and S.L.; methodology, L.L., H.S. and L.H.; validation, H.S., L.L. and L.H.; writing—original draft, L.L., L.H. and H.S.; writing—review and editing, L.L., X.W. and S.L. All authors have read and agreed to the published version of the manuscript.

Funding: This research was funded by the National Natural Science Foundation of China (Grant No. 42271405), the Science and Technology Department of Sichuan Province (Grant No. 2022NSFSC0231, 2023NSFSC0248), the National College Students Innovation and Entrepreneurship Training Program (Grant No. 202110616001) and the Provincial College Students Innovation and Entrepreneurship Training Program (Grant No. s202210616002).

Institutional Review Board Statement: Not applicable.

Informed Consent Statement: Not applicable.

Data Availability Statement: The data presented in this study are available on request from the corresponding author.

Acknowledgments: The authors are highly grateful for the support of the funds and projects and sincerely thank Shao for his guidance and support from beginning to end.

Conflicts of Interest: The authors declare no conflict of interest.

References

1. Zheng, H.; Li, Y.; Ouyang, Z.; Luo, Y. Progress and perspectives of ecosystem services management. *Acta Ecol. Sin.* **2013**, *33*, 702–710. [CrossRef]
2. Hu, W.; Li, G.; Gao, Z.; Ji, A.G.; Wang, Z.; Li, Y. Assessment of the impact of the Poplar Ecological Retreat Project on water conservation in the Dongting Lake wetland region using the InVEST model. *Sci. Total Environ.* **2020**, *733*, 139423. [CrossRef]
3. Zhang, M.; Zhao, Y.; Liu, F.; Pan, X. Glacier Dynamics and Water Balance in the Qinghai-Tibet Plateau. *Environ. Sci. Technol.* **2012**, *46*, 6449–6450. [CrossRef]
4. Wu, S.; Zhou, W.; Yan, K.; Zhang, X. Response of the Water Conservation Function to Vegetation Dynamics in the Qinghai-Tibetan Plateau Based on MODIS Products. *IEEE J. Sel. Top. Appl. Earth Obs. Remote Sens.* **2020**, *13*, 1675–1686. [CrossRef]
5. Jia, Y.; Yang, Q.; Hu, F.; Ju, Q.; Wang, G. Prospect and progress of water conservation capacity evaluation in a changing environment. *Hydro-Sci. Eng.* **2022**, *1*, 37–47.
6. Li, M.; Liang, D.; Xia, J.; Song, J.; Cheng, D.; Wu, J.; Cao, Y.; Sun, H.; Li, Q. Evaluation of water conservation function of Danjiang River Basin in Qinling Mountains, China based on InVEST model. *J. Environ. Manag.* **2021**, *286*, 112212. [CrossRef] [PubMed]
7. Wang, Y.; Ye, A.; Peng, D.; Miao, C.; Di, Z.; Gong, W. Spatiotemporal variations in water conservation function of the Tibetan Plateau under climate change based on InVEST model. *J. Hydrol. Reg. Stud.* **2022**, *41*, 101064. [CrossRef]
8. Zhang, X.; Li, Y.; Lv, C.; Bi, R.; Xia, L.; Guo, Y.; Wang, Y.; Xv, C.; Sun, B. Research progress on the application of ecosystem service functions based on the InVEST model. *Ecol. Sci.* **2022**, *41*, 237–242. [CrossRef]
9. Wang, Y.; Xv, P.; Xv, B.; Wang, W.; Wang, H. Water Conservation Function Assessment Models of Forest cosystem:A Review. *Ecol. Econ.* **2018**, *34*, 158–164, 169.
10. Govind, A.; Chen, J.M.; Margolis, H.; Ju, W.; Sonnentag, O.; Giasson, M.-A. A spatially explicit hydro-ecological modeling framework (BEPS-TerrainLab V2.0): Model description and test in a boreal ecosystem in Eastern North America. *J. Hydrol.* **2009**, *367*, 200–216. [CrossRef]
11. Xie, X.; Li, A.; Jin, H.; Bian, J.; Zhang, Z.; Nan, X. Comparing Three Remotely Sensed Approaches for Simulating Gross Primary Productivity over Mountainous Watersheds: A Case Study in the Wanglang National Nature Reserve, China. *Remote Sens.* **2021**, *13*, 3567. [CrossRef]
12. Zheng, X.; Chen, L.; Gong, W.; Yang, X.; Kang, Y. Evaluation of the Water Conservation Function of Different Forest Types in Northeastern China. *Sustainability* **2019**, *11*, 4075. [CrossRef]
13. Peng, Z.; Li, Y.; Yu, W.; Xing, Y.; Feng, A.; Du, S. Study on the Applicability of Remote Sensing Precipitation Products in Different Climate Zones in China. *J. Geo-Inf. Sci.* **2021**, *23*, 3498–3507. [CrossRef]
14. Li, Y.; Ma, X.; Qi, G.; Wu, Y. Studies on Water Retention Function of Anhui Province Based on InVEST Model of Parameter Localization. *Resour. Environ. Yangtze Basin* **2022**, *31*, 313–325.
15. Nie, Y.; Gong, B.; Yi, X. Water Conservation Valuation of Qinghai-Tibet Plateau. *Res. Soil Water Conserv.* **2009**, *16*, 210–212.
16. Long, D.; Li, X.; Li, X.; Han, P.; Zhao, F.; Hong, H.; Wang, Y.; Tian, F. Remote sensing retrieval of water storage hanges and underlying climatic echanisms over the Tibetan Plateau during 2000–2020. *Adv. Water Sci.* **2022**, *33*, 375–389.
17. Yin, Y.; Wu, S.; Zhao, D.; Dai, E. The impact of climate change on water conservation in the source area of the Yellow River in the past 30 years. *Geogr. Res.* **2016**, *35*, 49–57.
18. Zhang, J.; Liu, J.; Jin, J.; Ma, T.; Wang, G.; Liu, H.; Min, X.; Wang, H.; Lin, J.; Bao, Z.; et al. Evolution and Trend of Water Resources in Qinghai-Tibet Plateau. *Bull. Chin. Acad. Sci.* **2019**, *34*, 1264–1273.
19. Nie, Y.; Gong, B.; Li, Z. Spatio-temporal variation of water conservation capacity in the Qinghai-Tibet Plateau. *Earth Sci. Front. China Univ. Y Geosci. Beijing Peking Univ.* **2010**, *16*, 373–377.
20. Song, X.; Yan, C.; Xie, J.; Li, S. Assessment of changes in the area of the water conservation forest in the Qilian Mountains of China's Gansu province, and the effects on water conservation. *Environ. Earth Sci.* **2012**, *66*, 2441–2448. [CrossRef]
21. Niu, Y.; Li, S.; Liu, Y.; Shi, J.; Wang, Y.; Ma, Y.; Gao, L. Regulation of alpine meadow patch coverage on runoff and sediment under natural rainfall on the eastern Qinghai-Tibetan Plateau. *J. Hydrol.* **2021**, *603*, 127101. [CrossRef]
22. Hua, T.; Wang, X. Temporal and Spatial Variations in the Climate Controls of Vegetation Dynamics on the Tibetan Plateau during 1982–2011. *Adv. Atmos. Sci.* **2018**, *35*, 1337–1346. [CrossRef]
23. Taheri Dehkordi, A.; Valadan Zoej, M.J.; Ghasemi, H.; Ghaderpour, E.; Hassan, Q.K. A New Clustering Method to Generate Training Samples for Supervised Monitoring of Long-Term Water Surface Dynamics Using Landsat Data through Google Earth Engine. *Sustainability* **2022**, *14*, 8046. [CrossRef]
24. Chen, B.; Zhang, X.; Tao, J.; Wu, J.; Wang, J.; Shi, P.; Zhang, Y.; Yu, C. The impact of climate change and anthropogenic activities on alpine grassland over the Qinghai-Tibet Plateau. *Agric. For. Meteorol.* **2014**, *189–190*, 11–18. [CrossRef]
25. Pan, T.; Wu, S.; Liu, Y. Relative Contributions of Land Use and Climate Change to Water Supply Variations over Yellow River Source Area in Tibetan Plateau during the Past Three Decades. *PLoS ONE* **2015**, *10*, 373–377. [CrossRef] [PubMed]

26. Yang, J.; Xie, B.; Zhang, D.; Tao, W. Climate and land use change impacts on water yield ecosystem service in the Yellow River Basin, China. *Environ. Earth Sci.* **2021**, *80*, 1–12. [CrossRef]
27. Pan, T.; Wu, S.; Dai, E.; Liu, Y. Spatiotemporal variation of water source supply service in Three Rivers Source Area of China based on InVEST model. *Chin. J. Appl. Ecol.* **2013**, *24*, 183–189.
28. Zhao, Y.; Zhou, J.; Lei, L.; Xiang, J.; Huang, M.; Feng, W.; Zhu, G.; Wei, W.; Wang, J. Identification of drivers for water yield in the upstream of Shiyang River based on InVEST model. *Chin. J. Ecol.* **2019**, *38*, 3789–3799.
29. Liu, Y.; Li, Y.; Shan, S.; Yang, L.; Xu, H. Spatiotemporal variability in the water conservation amount in Gansu Qilian Mountain National Nature Reserve. *Pratacultural Sci.* **2021**, *38*, 1420–1431.
30. Xue, J.; Li, Z.; Feng, Q.; Miao, C.; Deng, X.; Di, Z.; Ye, A.; Gong, W.; Zhang, B.; Gui, J.; et al. Spatiotemporal variation characteristics of water conservation amount in the Qilian Mountains from 1980 to 2017. *J. Glaciol. Geocryol.* **2022**, *44*, 1–13.
31. Bao, Y.; Li, T.; Liu, H.; Ma, T.; Wang, H.; Liu, K.; Shen, Q.; Liu, X. Spatial-temporal variation of water conservation function in the Loess Plateau of northern Shaanxi based on InVEST model. *Geogr. Res.* **2016**, *35*, 664–676. [CrossRef]
32. Xie, Y.; Gong, J.; Qi, S.; Wu, J.; Hu, B. Spatial-temporal differentiation of water supply services in Bailongjiang River Basin based on InVEST model. *J. Nat. Resour.* **2017**, *32*, 1337–1347. [CrossRef]
33. Liu, J.; Fu, B.; Zhang, C.; Hu, Z.; Wang, Y. Water conservation capacity and value assessment of upper Min River ecosystem based on InVEST model. *Resour. Environ. Yangtze Basin* **2019**, *28*, 577–585.
34. Wang, G.; Han, D. Analysis of water production function in the upper reaches of Daling River based on InVEST model. *Yellow Rive R.* **2020**, *42*, 42–47.
35. Jia, W.; Wu, S.; Chen, A. Evaluation of ecosystem service functions in Chishui River Basin based on InVEST model. *J. China Inst. Water Resour. Hydropower Res.* **2020**, *18*, 313–320. [CrossRef]
36. Deng, R.; Shai, H.; Huang, B.; Zhang, C.; Zhou, Z.; Fan, J. Remote evaluation of ecosystem integrity and time sequence study of national park group construction on the Qinghai-Tibet Plateau. *Acta Ecol. Sin.* **2021**, *41*, 847–860.
37. Dai, E.; Wang, Y. Spatial heterogeneity and attribution analysis of water production services in Hengduan Mountain. *Acta Geogr. Sin.* **2020**, *75*, 607–619. [CrossRef]
38. Di, Y.; Zhang, Y.; Zeng, H.; Tang, Z. Effects of Changed Asian Water Tower on Tibetan Plateau Ecosystem: A Review. *Bull. Chin. Acad. Sci.* **2019**, *34*, 1322–1331.
39. Xu, X.; Chen, H.; Levy, J.K. K Spatial-temporal variation of vegetation cover characteristics of Qinghai-Tibet Plateau under climate warming and analysis of its causes. *Sci. China Press* **2008**, *53*, 456–462.
40. Sirigu, S.; Montaldo, N. Climate Change Impacts on the Water Resources and Vegetation Dynamics of a Forested Sardinian Basin through a Distributed Ecohydrological Model. *Water* **2022**, *14*, 3078. [CrossRef]
41. Zhao, S.; Fan, W.; Yu, N. Analysis of annual precipitation of Dong Zhiyuan based on wavelet and MK test. *J. Hebei Univ. Eng. Nat. Sci. Ed.* **2020**, *27*, 285–301.
42. Wang, X.; Ma, M.; Song, Y.; Tan, J.; Wang, H. Coupling of a biogeochemical model with a simultaneous heat and water model and its evaluation at an alpine meadow site. *Environ. Earth Sci.* **2014**, *72*, 4085–4096. [CrossRef]
43. Fu, B.; Ouyang, Z.; Shi, P.; Fan, J.; Wang, X.; Zheng, H.; Zhao, W.; Wu, F. Status of ecological security barrier and protection countermeasures on the Qinghai-Tibet Plateau. *Policy Manag. Res.* **2021**, *36*, 1298–1306. [CrossRef]
44. Gao, Q.; Miao, Y.; Song, J. Research progress on sustainable development of the Qinghai-Tibet Plateau. *Geogr. Res.* **2021**, *4*, 1–17. [CrossRef]
45. Dorje, L.L. Protection and utilization of water resources on the Qinghai-Tibet Plateau. *Resour. Sci.* **2005**, *27*, 23–27.
46. Lan, X.; Ye, C.; Wang, Y.; Zeng, T.; Sun, J. Spatio-temporal evolution characteristics and driving force analysis of water conservation function on the Tibetan Plateau from 1995 to 2014. *Acta Agrestia Sin.* **2021**, *29*, 80–92.
47. Liu, J.; Lang, X.; Su, J.; Liu, W.; Liu, H.; Tian, Y. Evaluation of water conservation function in the dry-hot valley area of Jinsha River Basin based on InVEST model. *Acta Ecol. Sin.* **2021**, *41*, 8099–8111.
48. Zhou, W.; Liu, G.; Pan, J. Empirical estimation of effective soil water content: A case study of Northeast Black Soil. *J. Arid Land Resour. Environ.* **2003**, *17*, 88–95.
49. Zhao, L.; Hu, G.; Zou, D.; Wu, X.; Ma, L.; Sun, Z.; Yuan, L.; Zhou, H.; Liu, S. Effects of Permafrost Changes on the Qinghai-Tibet Plateau on Hydrological Processes. *Change Asian Water Tower* **2019**, *34*, 1233–1246. [CrossRef]
50. Liljedahl, A.K.; Boike, J.; Daanen, R.P.; Fedorov, A.N.; Frost, G.V.; Grosse, G.; Hinzman, L.D.; Iijma, Y.; Jorgenson, J.C.; Matveyeva, N.; et al. Pan-Arctic ice-wedge degradation in warming permafrost and its influence on tundra hydrology. *Nat. Geosci.* **2016**, *9*, 312–318. [CrossRef]
51. Wu, P.; Liang, S.; Wang, X.-S.; McKenzie, J.M.; Feng, Y. Climate Change Impacts on Cold Season Runoff in the Headwaters of the Yellow River Considering Frozen Ground Degradation. *Water* **2020**, *12*, 602. [CrossRef]
52. Liu, Z.; Li, S.; Wei, W.; Song, X. Research progress on wetland changes and driving forces on the Qinghai-Tibet Plateau in the past three decades. *Chin. J. Ecol.* **2019**, *38*, 856–862.
53. Duan, H.; Xue, X.; Wang, T.; Kang, W.; Liao, J.; Liu, S. Spatial and Temporal Differences in Alpine Meadow, Alpine Steppe and All Vegetation of the Qinghai-Tibetan Plateau and Their Responses to Climate Change. *Remote Sens.* **2021**, *13*, 669. [CrossRef]
54. Shi, W.; Qiao, F.; Zhou, L. Identification of Ecological Risk Zoning on Qinghai-Tibet Plateau from the Perspective of Ecosystem Service Supply and Demand. *Sustainability* **2021**, *13*, 5366. [CrossRef]

55. Liu, X.; Chen, Y.; Li, Z.; Li, Y.; Zhang, Q.; Zan, M. Driving Forces of the Changes in Vegetation Phenology in the Qinghai-Tibet Plateau. *Remote Sens.* **2021**, *13*, 4952. [CrossRef]
56. Chen, H.; Ouyang, W.; Lv, F.; Song, Y.; Hao, R. Variation of Vegetation Cover and Its Correlation of Topographic Factors in Guandu River Basin. *Res. Soil Water Conserv.* **2019**, *26*, 135.
57. Ghaderpour, E.; Mazzanti, P.; Mugnozza, G.S.; Bozzano, F. Coherency and phase delay analyses between land cover and climate across Italy via the least-squares wavelet software. *Int. J. Appl. Earth Obs. Geoinf.* **2023**, *118*, 103241. [CrossRef]
58. Liu, J.; Ji, Y.; Zhou, G.; Zhou, L.; Lyu, X.; Zhou, M. Temporal and spatial variations of net primary productivity (NPP) and its climate driving effect in the Qinghai-Tibet Plateau, China from 2000 to 2020. *Chin. J. Appl. Ecol.* **2022**, *33*, 1533–1538. [CrossRef]
59. Xv, Y.; Huang, W.; Dou, S.; Guo, Z.; Li, X.; Zheng, Z.; Jing, J. Responding Mechanism of Vegetation Cover to Climate Change and Human Activities in Southwest China from 2000 to 2020. *Environ. Sci.* **2022**, *43*, 3230–3240. [CrossRef]
60. Zhang, X.; Lu, L.; Yu, H.; Zhang, X.; Li, D. Multi-scenario simulation of the impact of land use change on the value of ecosystem services on the Qinghai-Tibet Plateau. *Chin. J. Ecol.* **2021**, *40*, 992.
61. Gao, Y.; Huang, J.; Li, S.; Li, S. Spatial pattern of non-stationarity and scale-dependent relationships between NDVI and climatic factors—A case study in Qinghai-Tibet Plateau, China. *Ecol. Indic.* **2012**, *20*, 170–176. [CrossRef]
62. Wang, H.; Qi, Y.; Huang, C.; Li, X.; Deng, X.; Zhang, J. Analysis of vegetation changes and dominant factors on the Qinghai-Tibet Plateau, China. *Sci. Cold Arid Reg.* **2019**, *11*, 150–158. [CrossRef]
63. Chen, C.; Li, T.; Sivakumar, B.; Sharma, A.; Albertson, J.D.; Zhang, L.; Wang, G. Combined Effects of Warming and Grazing on Rangeland Vegetation on the Qinghai-Tibet Plateau. *Front. Environ. Sci.* **2021**, *9*, 797971. [CrossRef]
64. Sun, L.; Li, H.; Wang, J.; Chen, Y.; Xiong, N.; Wang, Z.; Wang, J.; Xu, J. Impacts of Climate Change and Human Activities on NDVI in the Qinghai-Tibet Plateau. *Remote Sens.* **2023**, *15*, 587. [CrossRef]
65. Cao, Y.; Sun, M.; Chen, M.; He, Y.; Song, H. Effects of precipitation on vegetation cover in the northern Tibetan Plateau from 2000 to 2016. *Acta Ecol. Sin.* **2022**, *30*, 721–730.
66. Wang, L.; Wei, X.; Zhang, Z.; Guo, Z.; Huang, S. Changes of vegetation index in Qinghai-Tibet Plateau and its relationship with temperature and humidity factors. *J. For. Environ.* **2022**, *42*, 141–148.
67. Guo, X.; Song, H.; Zhai, L. Spatial-temporal variation characteristics of vegetation cover on the Qinghai-Tibet Plateau and its driving factors. *Chin. J. Ecol.* **2022**, 1–13. Available online: http://kns.cnki.net/kcms/detail/21.1148.Q.20221228.1533.009.html (accessed on 1 April 2023).
68. Ouyang, X.; Dong, X.; Wei, R.; Gong, C.; Wu, H. Spatial-temporal variation of NDVI in vegetation growing season on the Qinghai-Tibet Plateau and its response to climatic factors. *Res. Soiland Water Conserv.* **2023**, *30*, 220–229. [CrossRef]
69. Li, W.; Xv, J.; Yao, Y.; Zhang, Z. Temporal and spatial variation characteristics of vegetation index (NDVI) in the Sanjiangyuan area of the Qinghai-Tibet Plateau under the background of global warming. *Mt. Res.* **2021**, *39*, 473–482.
70. Cai, L.; Tian, L.; Ao, Y.; Wang, X. Influence of human disturbance on vegetation cover change on the Qinghai-Tibet Plateau. *Res. Soil Water Conserv.* **2021**, *28*, 382–388. [CrossRef]
71. Kumari, N.; Saco, P.M.; Rodriguez, J.F.; Johnstone, S.A.; Srivastava, A.; Chun, K.P.; Yetemen, O. The Grass Is Not Always Greener on the Other Side: Seasonal Reversal of Vegetation Greenness in Aspect—Driven Semiarid Ecosystems. *Geophys. Res. Lett.* **2020**, *47*, e2020GL088918. [CrossRef]
72. Matsushita, B.; Yang, W.; Chen, J.; Onda, Y.; Qiu, G. Sensitivity of the Enhanced Vegetation Index (EVI) and Normalized Difference Vegetation Index (NDVI) to Topographic Effects: A Case Study in High-density Cypress Forest. *Sensors* **2007**, *7*, 2636–2651. [CrossRef] [PubMed]
73. Yang, X.; Zuo, X.; Xie, W.; Li, Y.; Guo, S.; Zhang, H. A Correction Method of NDVI Topographic Shadow Effect for Rugged Terrain. *IEEE J. Sel. Top. Appl. Earth Obs. Remote Sens.* **2022**, *15*, 8456–8472. [CrossRef]
74. Xiao, X.; Qiu, X.; Xv, J. Characteristics of wet and dry climate change in China from 1960 to 2019 based on the TerraClimate dataset. *J. Chang. River Sci. Res. Inst.* **2023**, *40*, 27–33.
75. Abatzoglou, J.T.; Dobrowski, S.Z.; Parks, S.A.; Hegewisch, K.C. TerraClimate, a high-resolution global dataset of monthly climate and climatic water balance from 1958–2015. *Sci Data* **2018**, *5*, 170191. [CrossRef] [PubMed]